Arabian Journal of Chemistry (2023) **16**, 104603

King Saud University

Arabian Journal of Chemistry

www.ksu.edu.sa
www.sciencedirect.com

ORIGINAL ARTICLE

A dual-functional chemosensor based on acylhydrazone derivative for rapid detection of Zn (II) and Mg(II): Spectral properties, recognition mechanism and application studies

Yongjie Ding [a,c], Chunxiang Zhao [a,*], Pengcheng Zhang [a], Yahong Chen [b,*], Jianping Xie [a], Weiwu Song [b], Zengchen Liu [c], Guanglu Liu [c], Xinyu Zheng [a]

[a] *College of Chemistry and Chemical Engineering, Zhoukou Normal University, Zhoukou, Henan 466001, China*
[b] *Zhoukou Key Laboratory of Small Molecule Drug Development and Application, Zhoukou 466001, China*
[c] *Institute of Medicinal Development and Application for Aquatic Disease Control, Zhoukou Normal University, Zhoukou 466001, China*

Received 22 October 2022; accepted 15 January 2023
Available online 21 January 2023

KEYWORDS

Acylhydrazone;
Dual-functional chemosensor;
Zinc ion;
Magnesium ion;
Theoretical calculations;
Application

Abstract In this work, an acylhydrazone derivative (**QN62**) was developed via the one-step condensation of 6-hydroxy-2-naphthoic hydrazide with quinoline-8-carboxaldehyde. The structure of the **QN62** compound was characterized by ^{1}H NMR, ^{13}C NMR, HR-MS (ESI), and X-ray crystallography. As a dual-functional turn-on fluorescence chemosensor, **QN62** exhibited rapid recognition for Zn^{2+} in DMSO-H_2O (4:1, v/v) and Mg^{2+} in ethanol-H_2O (9:1, v/v). The enhancement in fluorescence detection was associated with the coordination reaction between **QN62** and the target ions, which promoted intramolecular charge transfer and prevented the C═N isomerization process. Simultaneously, a rapid color change from colorless to yellowish-green or yellow under UV light (365 nm) was easily visible to the naked eye. Under optimal conditions, the limit of detection and limit of quantification were 32.3 nM and 97.8 nM for Zn^{2+} and 16.1 nM and 48.9 nM for Mg^{2+}, respectively. The recognition mechanism was reasonably speculated based on analysis of the Job's plot, HR-MS, ^{1}H NMR, and density functional theoretical calculations. Utilizing silica-gel plates fabricated from the **QN62** chemosensor, the visual and rapid identification of Zn^{2+} and Mg^{2+} was successfully achieved, which could provide a convenient approach for on-site detection in environmental fields. The **QN62** chemosensor could also quantify trace amounts of Zn^{2+} and

* Corresponding authors.
E-mail addresses: zcx@zknu.edu.cn (C. Zhao), 20041023@zknu.edu.cn (Y. Chen).
Peer review under responsibility of King Saud University.

Production and hosting by Elsevier

https://doi.org/10.1016/j.arabjc.2023.104603
1878-5352

Mg^{2+} in water samples. Furthermore, the cell imaging experiments indicated that **QN62** could effectively sense intracellular Zn^{2+} and Mg^{2+}, providing potential applications in biological systems.

1. Introduction

The abnormal accumulation of metal ions can cause potential hazards for the biological environment and human health (Geng, et al., 2022; Sidqi, et al., 2022; Aysha, et al., 2021). For example, Zn^{2+} plays a vital role in many biological processes such as signal transduction, cellular metabolism, and gene expression, but zinc homeostasis disturbances may be responsible for neurodegenerative syndromes (Maity, et al., 2019; Wang, et al., 2022; Bush, et al., 1994). In the environment, high concentrations of zinc (1300 mg/kg) can diminish soil microbial activity, resulting in phytotoxic effects (Voegelin, et al., 2005; Moreno, et al., 2009). Similarly, as a significant element in living beings and the environment, magnesium imbalances may also induce various diseases, including hypermagnesemia, diarrhea, and metabolic syndrome (Fu, et al., 2021; Matsui, et al., 2017). Thus, developing efficient and convenient methods for detecting trace metal ions has attracted widespread attention.

Fluorescence-based molecular probes have been extensively investigated for the recognition of trace metal ions due to their unique superior characteristics, such as fast response, good selectivity, high sensitivity, low detection limit, and operational simplicity (Saravana Kumar, et al., 2020; Jiang, et al., 2019). Abundant fluorescent probes have been shown to be efficient for detecting single metal ions such as Zn^{2+} (Bumagina, et al., 2022), Al^{3+} (Kolcu and Kaya, 2022), Hg^{2+} (Musikavanhu, et al., 2022; Mohamed, et al., 2022), Cu^{2+} (Ahmed, et al., 2022; Picci, et al., 2021; Khan, et al., 2022), Mg^{2+} (Hu, et al., 2017), Cd^{2+} (Mohanasundaram, et al., 2021), and Cr^{3+} (Khan, et al., 2022). The development of dual-functional chemosensors has also attracted great interest among researchers, as dual chemosensors can identify-two species, effectively saving time and costs compared to one-to-one detection probes (Hazra, et al., 2018; Roy, et al., 2021; Alam, et al., 2016; Anbu, et al., 2014; Gogoi, et al., 2014; Dong, et al., 2017). So far, a small number of fluorescent probes have been reported for the simultaneous detection of Zn^{2+} and Mg^{2+} ions. For example, a Schiff-base compound based on coumarin was prepared for the sensing of Zn^{2+} and Mg^{2+}, showing significant enhancement of the fluorescence peaks at 558 nm for Zn^{2+} and 550 nm for Mg^{2+} (λ_{ex} = 450 nm) (Maity and Bharadwaj, 2014). Alam et al. (Alam, et al., 2014) reported on a quinoline derivative as a turn-on fluorescent probe for Zn^{2+} and Mg^{2+}, which exhibited emissions at 539 nm for Zn^{2+} and 526 nm for Mg^{2+} (λ_{ex} = 430 nm). An acylhydrazone compound based on naphthalene and pyrazole, developed by Dhara et al. (Dhara, et al., 2016), was used as a dual sensor for Zn^{2+} and Mg^{2+} ions. In the complexation studies, the amide carbonyl O and pyrazole N atoms acted as metal binding sites to form 1:1 complexes. Wang et al. (Wang, et al., 2019) reported on isoquinoline-based acylhydrazone, which could efficiently recognize Zn^{2+} and Mg^{2+} by altering the solvent from DMF-H_2O (9:1, v/v) to acetonitrile. However, some of the reported probes showed certain limitations as overlapping response signals, low sensitivity, or a multi-step synthetic route. Thus, there is scope for modulating dual chemosensor properties utilizing the selective combination of organic functional groups (Wang, et al., 2019).

Quinolines have been widely utilized as fluorophores for constructing probes due to their unique advantages of good biocompatibility, easy structural modification, and stable photophysical properties (Wang, et al., 2021; Xu, et al., 2022; Yan, et al., 2021). The nitrogen atom in the quinoline group can also be used as a binding site for coordination with metal ions, accompanied by the enhancement of fluorescence quantum yield (Wang, et al., 2021). In addition, naphthalenes are well-known, ideal fluorophores in the design of fluorescent chemosensors. An electron donating group and an electron withdrawal group have been introduced into the 2- and 6-positions of naphthalene to provide a push–pull electronic system, possessing intramolecular charge transfer (ICT) characteristics (Sun, et al., 2020; Li, et al., 2019). Moreover, acylhydrazone backbones have shown a strong coordination ability with metal ions through the N atom of imine and the O atom of carbonyl (Liao, et al., 2017). After binding with certain metal ions, acylhydrazone-based probes usually display a turn-on fluorescence response by restricting the free rotation of -C═N (Sun, et al., 2020).

Combining the advantages of the above functional groups, and to further continue our study on the development of dual chemosensors (Ding, et al., 2021), in this work, we rationally designed and developed a simple acylhydrazone chemosensor (**QN62**) through a one-step condensation reaction between 6-hydroxy-2-naphthoic hydrazide and quinoline-8-carboxaldehyde. In this work, **QN62** could discriminate between Zn^{2+} in DMSO-H_2O (4:1, v/v) medium and Mg^{2+} in ethanol-H_2O (9:1, v/v) medium, showing significant fluorescence enhancement. The response mechanism of **QN62** to Zn^{2+}/Mg^{2+} was investigated by fluorescence measurements, HR-MS, ^{1}H NMR, and theoretical calculations. The designed compound **QN62** achieved visual and rapid identification of the target ions using silica-gel plates. Moreover, it was successfully used to quantify trace amounts of Zn^{2+} and Mg^{2+} in water samples and readily sensed intracellular Zn^{2+} and Mg^{2+}, which could be used as a guideline for future detection in environmental and biological systems.

2. Experimental

2.1. Materials and instruments

All of the reagents and chemicals used in this study were of analytical grade and used without further purification. Quinoline-8-carboxaldehyde was purchased from Energy Chemical (Shanghai, China), 6-hydroxy-2-naphthoic hydrazide was purchased from J&K Scientific ltd. (Beijing, China), and all other reagents were purchased from Sinopharm Chemical (Shanghai, China). The melting point was determined by a Beijing XT4-100x microscopic melting point apparatus (Beijing Electrooptical Instrument Factory, China). The ^{1}H NMR and ^{13}C NMR spectra were measured by a Bruker AV-500 spectrometer (Bruker BioSpin Gmbh, Germany), the Fourier transform infrared (FT-IR) spectra were obtained on a Nicolet 6700 spectrometer (Thermo Fisher Scientific, USA), and the high-resolution mass spectra (HR-MS) spectra were obtained using a UPLC G2-XS mass spectrometer (Waters, USA). A TU-1901 UV–vis spectrophotometer (PGeneral Instrument Inc., China) and Cary Eclipse fluorescence spectrofluorometer (Agilent Technologies, USA) were used to measure absorption and fluorescent spectra, and the cell imaging experiments were observed by an Olympus FV3000 confocal laser-scanning microscope (Olympus FV3000, Japan).

A Bruker Smart CCD single-crystal diffractometer (Bruker AXS GmbH, Germany) was utilized to collect single crystal data. Measurement was performed at 173 K using a graphite monochromated Mo-Kα radiation (λ = 0.71073 Å). SHELXS-97 program was used to solve and refine the crystal structure by full-matrix least-squares techniques on F^2 (Sheldrick, 1997). The structure plots was used Diamond software (Brandenburg, 2012). Crystallographic data CCDC2192938 for the structure **QN62** has been deposited with the Cambridge Crystallographic Data Centre and can be obtained free of charge via https://www.ccdc.cam.ac.uk.

2.2. Synthesis of compound QN62

The compound 6-hydroxy-*N'*-(quinolin-8-ylmethylene)naphthalene-2-carbohydrazide (**QN62**) was prepared as follows, quinoline-8-carboxaldehyde (250 mg, 1.60 mmol) was dissolved in 20 mL of 1,4-dioxane and then 6-hydroxy-2-naphthoic hydrazide (320 mg, 1.60 mmol) was added. After refluxed for 4 h, the solvent was removed under reduced pressure and the crude product was purified by column chromatography on silica gel (dichloromethane-methanol, 9:1, v/v). Crystallization from dichloromethane-methanol (4:1, v/v) gave fusiform yellow single crystals. Yield: 78 %. m.p.: 164.5–165.5 °C. IR (cm^{-1}) (Fig. S1): 3453 (–OH), 3200 (–NH), 3043 (HC =), 1629 (C═O), 1578 (C═N), 1288 (C─N, amide III band), 1215(C─O). ^{1}H NMR (500 MHz, DMSO d_6, ppm) (Fig. S2): 12.20(1H, s, OH), 10.15(1H, s, NH), 9.80(1H, s,–CH = N), 9.01(1H, dd, J = 4.1, 1.7 Hz, ArH), 8.53(1H, s, ArH), 8.47(1H, m, ArH), 8.43(1H, d, J = 7.2 Hz, ArH), 8.10(1H, d, J = 8.0 Hz, ArH), 8.01–7.91(2H, m, ArH), 7.82 (1H, d,J = 8.6 Hz, ArH), 7.74(1H, t, J = 7.7 Hz, ArH), 7.64(1H, dd, J = 8.3, 4.1 Hz, ArH), 7.25–7.17(2H, m, ArH). ^{13}C NMR (125 MHz, DMSOd_6, ppm) (Fig. S3): 163.12, 157.08, 150.27, 145.27, 144.20, 136.62, 136.27, 131.25, 130.69, 129.87, 128.11, 127.98, 127.14, 126.52, 126.08, 125.53, 124.53, 121.83, 119.47, 108.59. ESI-Mass (Fig. S4): m/z calcd. for [**QN62** + H]$^+$, 342.1198; found, 342.1242.

2.3. Spectroscopic measurements

The **QN62** stock solution (1.0 mM) was prepared in THF. Various solutions of metal ions (5.0 mM) were prepared by dissolving their nitrate or chloride salts in double distilled water. Test solutions were prepared with **QN62** stock solution (100 μL) and a certain volume of metal ions solution, and the mixture was diluted to 5 mL by DMSO-H_2O (4:1, v/v) or ethanol-H_2O (9:1, v/v). Different pH of solutions was adjusted with 1.0 mM NaOH or HCl. All experiments and test procedures were performed at room temperature.

2.4. Binding constant determination

The binding constant K of complexes was determined based on the modified Benesi-Hildebrand in Eq. (1) (Zhang, et al., 2018).

$$(Fmax - F0)/(Fx - F0) = 1 + 1/K[M] \quad (1)$$

where F_x and F_0 are the fluorescence intensity of **QN62** in the presence and absence of Zn^{2+}/Mg^{2+}, respectively, F_{max} is the maximal fluorescence intensity of **QN62** in the presence of Zn^{2+}/Mg^{2+} at saturation. [M] is the concentration of Zn^{2+} or Mg^{2+}.

2.5. Limit of detection (LOD) and limit of quantification (LOD) calculations

The limit of detection (LOD) and limit of quantification (LOQ) were calculated using the Eq. (2) and Eq. (3) (Goncalves, et al., 2022).

$$LOD = 3.3\sigma/k \quad (2)$$

$$LOQ = 10\sigma/k \quad (3)$$

where σ corresponds to the standard deviation of the blank sample, k is the slope of the fit lines in fluorescence titration.

2.6. Quantum yield measurement

The fluorescence quantum yield was estimated using anthracene (Φ_R = 0.27 in ethanol) (Rurack, 2008) as reference and using the following Eq. (4) (Immanuel David, et al., 2022).

$$\phi = \phi_R \times F/F_R \times A_R/A \times h^2/h_R^2 \quad (4)$$

where Φ is the quantum yield, F is the area of the fluorescence spectrum, A is the absorbance at the excitation wavelength and η is refractive index of solvent.

2.7. Cell imaging experiment

The MCF-7 cells were cultured with Dulbecco's modified Eagle's medium (DMEM) medium at 37℃ in a humidified incubator with 5 % CO_2. The cells were first incubated with 10 μM **QN62** at 37 °C for 30 min and washed three times to remove the excess of **QN62**. Subsequently, the cells were exposed to 10 μM Zn^{2+}/Mg^{2+} for 30 min under the same conditions. The fluorescence imaging of **QN62** in MCF-7 cells was carried out on a confocal laser scanning microscope.

3. Results and discussion

3.1. Characterization of Chemosensor QN62

The chemosensor **QN62** was synthesized as shown in Scheme 1. The target compound **QN62** was confirmed by FT-IR, ^{1}H NMR, ^{13}C NMR, and HR-MS analyses, as well as by single crystal X-ray diffraction. The characteristic absorption band –CH = N- at 1578 cm^{-1} appeared in the FT-IR spectrum of **QN62** (Fig. S1). In the ^{1}H NMR and ^{13}C NMR spectra of **QN62**, the proton and carbon signals of Schiff base CH = N resonated at their expected frequency ranges of 9.807 and 157.075 ppm, respectively (Fig. S2 and S3). In the HR-MS spectrum, the base peak was found at 342.1242 (calcd.

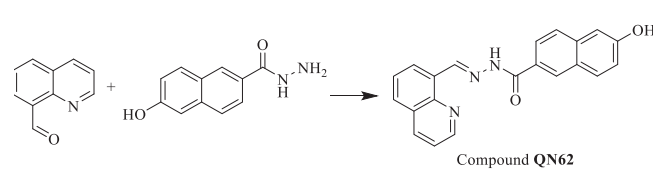

Scheme 1 Synthesis of compound **QN62.**

342.1198), corresponding to [**QN62** + H]$^+$ (Fig. S4). Moreover, the structure of compound **QN62** was explicitly established by X-ray crystallography. As shown in Fig. 1a, the quinoline unit and naphthalene ring of **QN62** were not in the same plane, presenting a dihedral angle of 13.87°. The lattice consisted of one **QN62** unit, which incorporated one disordered dichloromethane solvent molecule (Fig. 1a), and the crystalline lattice contained intermolecular O—H⋯O and N—H⋯O hydrogen bonds (Fig. 1b). Centro-symmetrically related molecules were connected into ring $R_2^2(20)$ dimers by intermolecular N(3)-H(3)⋯O(2) hydrogen bonds and the dimers were further linked by intermolecular O(2)-H(2)⋯O(1) hydrogen bonds, which formed an undulating two-dimensional network (Fig. 1c). The intermolecular hydrogen bonds played a key role in the formation of crystalline solids (Shyamsivappan, et al., 2020). The **QN62** compound for the crystallographic data, the selected bond lengths, and the bond angles were illustrated in Tables S1, S2, and S3, respectively.

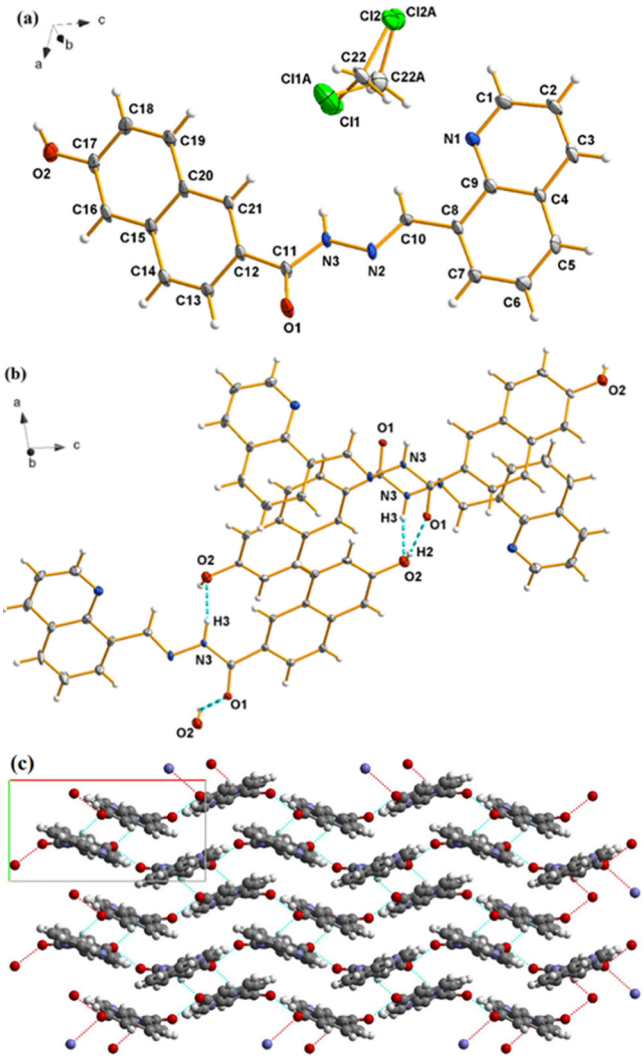

Fig. 1 (a) Ortep view of **QN62** drawn in 30 % probability thermal-displacement ellipsoids with the atom numbering scheme. (b) Part of the crystal structure of **QN62** showing the intermolecular hydrogen bonds (dotted lines). (c) two-dimensional undulating structure of **QN62**. H-bonds are shown by dotted lines.

3.2. Spectroscopic recognition of Zn^{2+} and Mg^{2+}

The fluorescent properties of chemosensor **QN62** were investigated in a series of solvents, including acetonitrile, ethanol, DMF, and DMSO. In the above solvents, **QN62** exhibited very weak fluorescence emissions (Fig. S5). In the designed **QN62** molecule, the combination of 6-position phenolic hydroxyl and 2-position acylhydrazone of naphthalene synergistically created a push–pull system, which possessed ICT features (Kim and Kim, 2021) and could be visualized by density functional theory (DFT) calculations, as presented later. Simultaneously, the isomerization of the -C═N- unit in the molecule easily underwent nonradiative deactivation of the excited states (Sivakumar and Lee, 2021). Thus, weak fluorescence was possibly caused by the synergistic contribution of C═N isomerization and the ICT process. In the above organic solvents, the fluorescence behavior of **QN62** toward common metal ions, including Ag^+, Al^{3+}, Ca^{2+}, Cd^{2+}, Co^{2+}, Cr^{3+}, Cu^{2+}, Fe^{2+}, Fe^{3+}, Hg^{2+}, K^+, Mg^{2+}, Na^+, Ni^{2+}, Zn^{2+} and Pb^{2+} was measured. A dramatic enhancement in the fluorescence signals was observed only at 532 nm with the addition of Zn^{2+} in DMSO-H_2O (4:1, v/v) media, and at 527 nm with Mg^{2+} in ethanol-H_2O (9:1, v/v) solution (Fig. 2). With the addition of 1.0 equiv. Zn^{2+} and Mg^{2+} ions to the respective analytical systems, the enhancements in **QN62** emission intensity were nearly 10-fold and 70-fold, respectively, and the fluorescence quantum yield also increased from 0.013 to 0.11 and 0.43. Other tested ions did not produce any obvious changes in the fluorescence emissions of **QN62** under identical conditions. Interfering congeners Cd^{2+}/Ca^{2+} exhibited minimal emission in the respective analyte system of Zn^{2+}/Mg^{2+}. Simultaneously, the colorless **QN62** solution changed to yellowish-green/yellow in the presence of Zn^{2+}/Mg^{2+} under irradiation of the 365 nm UV lamp, which was easily visible to the naked eye (Fig. 2. inset). These indicated that **QN62** could serve as an excellent fluorescent probe for Zn^{2+} and Mg^{2+} by switching solvents. The enhanced fluorescence response of **QN62** toward Zn^{2+}/Mg^{2+} was possibly due to the interactions of the metal ions with the binding sites, which increased the electron withdrawal ability of the coordinating groups, and this was further beneficial for the ICT process (Sivakumar and Lee, 2021; Hossain, et al., 2017). The restriction of -C═N- isomerization also played an essential role in the fluorescence enhancement process (Wu, et al., 2018).

The response time of **QN62** to detect Zn^{2+}/Mg^{2+} was studied. As shown in Fig. S6, the fluorescence intensity of **QN62** treated with Zn^{2+}/Mg^{2+} rapidly reached saturation within 2 min and then remained unchanged for 30 h. This performance could potentially provide a real-time detection method for Zn^{2+}/Mg^{2+} ions.

Due to the high fluorescence sensing ability of **QN62** toward Zn^{2+}/Mg^{2+} in DMSO/ethanol solution, the UV absorption spectral response of **QN62** before and after Zn^{2+}/Mg^{2+} addition was further investigated (Fig. 3). The **QN62** compound displayed a broad absorption band centered at 343 nm in DMSO-H_2O (4:1, v/v) and ethanol-H_2O (9:1, v/v) solutions, and the longer wavelength absorption band of **QN62** could be assigned to π-π* and n-π* charge transfer (CT) transitions (Djouhra, et al., 2017; Xie, et al., 2018). Upon the addition of Zn^{2+}/Mg^{2+}, the absorption band at 343 slightly decreased, accompanied by new bands at 400 nm for

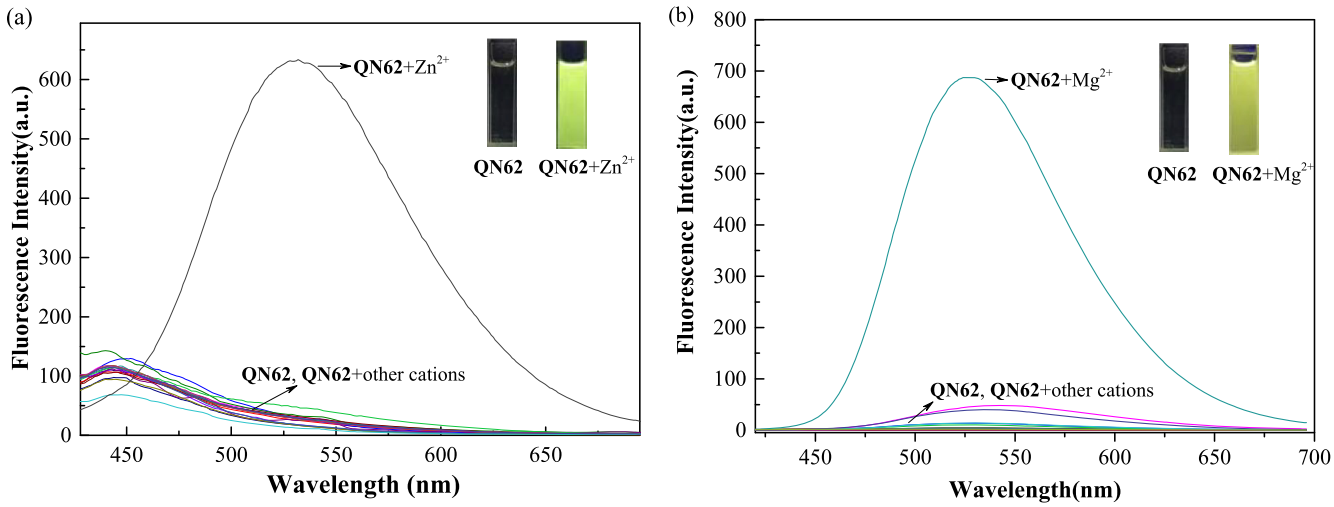

Fig. 2 (a) Fluorescence responses of **QN62** (20 μM) with different metal ions (20 μM) in DMSO-H_2O (4:1, v/v) (λex = 400 nm). (b) Fluorescence responses of **QN62** (20 μM) with different metal ions (20 μM) in ethanol-H_2O (9:1, v/v) (λex = 385 nm). Inset: images of **QN62** before and after addition of Zn^{2+}/Mg^{2+} under 365 nm UV-light.

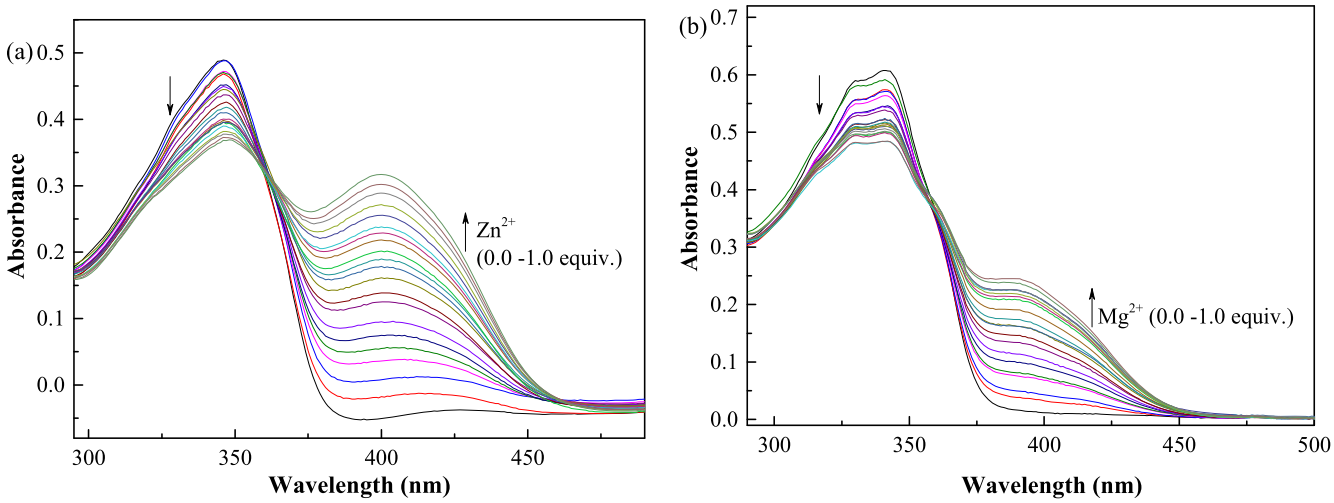

Fig. 3 (a) Change in the absorption spectral of **QN62** (20 μM) upon addition of Zn^{2+} (0–20 μM) in DMSO-H_2O (4:1, v/v). (b) Change in the absorption spectral of **QN62** (20 μM) upon addition of Mg^{2+} (0–20 μM) in ethanol-H_2O (9:1, v/v).

Zn^{2+} and 386 nm for Mg^{2+}, indicating the coordination reaction between **QN62** and Zn^{2+}/Mg^{2+}. After adding Zn^{2+}/Mg^{2+}, the red shifts of the absorption peaks of compound **QN62** were due to intramolecular charge transfer (Purkait, et al., 2019).

To extend the practical applicability of compound **QN62**, we investigated the fluorescence response of compound **QN62** before and after Zn^{2+}/Mg^{2+} addition at various pH values (Fig. S7). The experimental results showed that the fluorescence intensity of **QN62** did not change under acidic, neutral, or alkaline conditions. However, after adding Zn^{2+}/Mg^{2+}, the chemosensor **QN62** displayed notable emission enhancement under neutral and weakly alkaline conditions (pH 6–10 for Zn^{2+}, pH 6–9 for Mg^{2+}). In neutral and weakly alkaline conditions, the deprotonation process of **QN62** enhanced the electron-donating ability of phenolic O^-, producing a stronger binding affinity toward Zn^{2+}/Mg^{2+} ions (Khan, et al., 2022). A pH value of 7.0 was selected as the experimental condition, which was within the biologically relevant pH range (5.5–7.5) (Shi, et al., 2013; Xu, et al., 2017).

To determine the sensitivity of the **QN62** chemosensor for Zn^{2+}/Mg^{2+}, fluorometric titration was carried out (Fig. 4). The fluorescence intensity increased with a gradual increase in Zn^{2+}/Mg^{2+} concentration and was saturated at 1.0 equiv. Zn^{2+}/Mg^{2+}. Moreover, the fluorescence intensities at 532 nm and 527 nm showed a good linear relationship with the Zn^{2+} and Mg^{2+} concentrations in the range of 0.0–1.0 equiv. (Fig. S8). These results indicated that the **QN62** chemosensor could provide a potential method for the quantitative determination of Zn^{2+} and Mg^{2+}. The binding constant (K) values of the complexes were calculated to be 8.29×10^4 M^{-1} for Zn^{2+} and 6.34×10^4 M^{-1} for Mg^{2+} (Fig. S9), which were comparable to previously reported probes for Zn^{2+} and Mg^{2+} (Dhara, et al., 2016; Sun, et al., 2020). The large binding

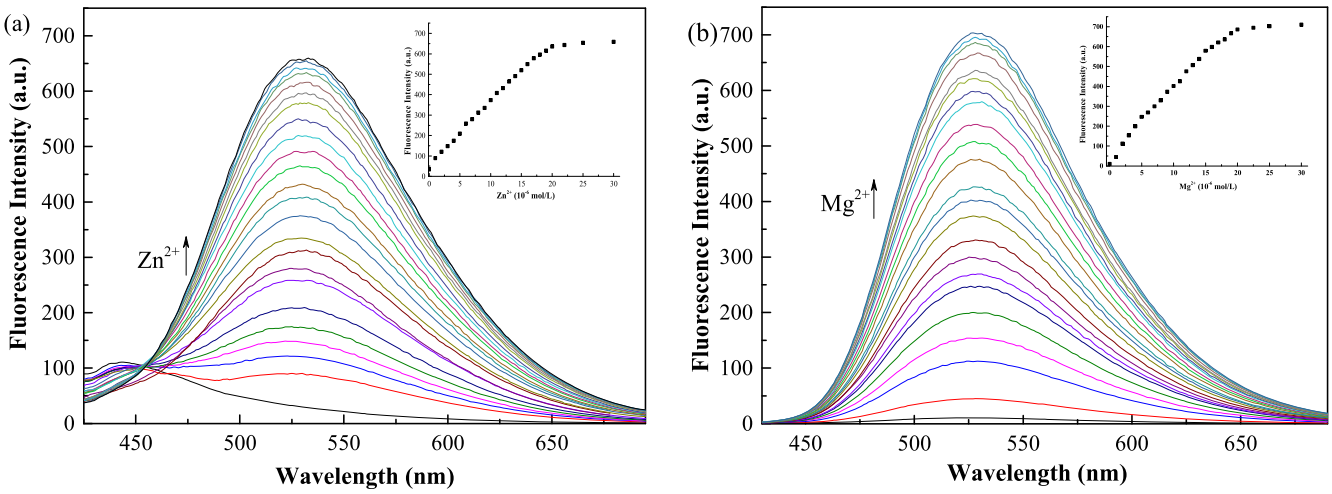

Fig. 4 (a) Emission spectral changes of compound **QN62** (20 μM) with increasing concentration of Zn^{2+}: 0–30 μM in DMSO-H_2O (4:1, v/v). (b) Emission spectral changes of compound **QN62** (20 μM) with increasing concentration of Mg^{2+}: 0–30 μM in ethanol-H_2O (9:1, v/v).

constant values suggested **QN62**-Zn^{2+}/**QN62**-Mg^{2+} complex formation (Jana, et al., 2016). The LOD values were calculated to be 32.3 nM for Zn^{2+} and 16.1 nM for Mg^{2+}, which were low compared with the reported Zn^{2+}/Mg^{2+} fluorescent probe (Table 1). Meanwhile, the LOQ values were also estimated to be 97.8 nM for Zn^{2+} and 48.9 nM for Mg^{2+}. The values of LOD and LOQ were below the WHO recommended limit of Zn^{2+} (5 mg/L) and Mg^{2+} (30 mg/L) for drinking water and were lower than the total Zn^{2+} concentrations (200–300 μM) and Mg^{2+} concentrations (200–1000 μM) in human cells (Wang, et al., 2021; Kumar and Puri, 2012; Maret, 2015; Farruggia, et al., 2006).

The selectivity of **QN62** for Zn^{2+}/Mg^{2+} mixed with other metal ions was examined by fluorescent competition experiments. As illustrated in Fig. S10a, except for Cu^{2+}, Co^{2+}, Fe^{3+}, Al^{3+}, and Cr^{3+}, the coexistence of other competitive ions showed minimal interference on the fluorescence intensity of the **QN62**-Zn^{2+} complex in DMSO-H_2O (4:1, v/v). The strong Lewis acidity of Al^{3+}, Cr^{3+}, and Fe^{3+} reduced the binding affinity of imine and phenolic hydroxyl groups towards the Zn^{2+} ion. In the case of Cu^{2+} and Co^{2+}, the high coordination affinity and their inherent magnetic properties resulted in a decrease in fluorescence emission intensity at 532 nm (Gao, et al., 2020). Although Co^{2+}, Fe^{3+}, Al^{3+}, and Cr^{3+} could cause interference with Zn^{2+} recognition, **QN62** still displayed an obvious enhancement of fluorescence intensity, which could effectively sense the target ion. When **QN62** acted as a magnesium ion in the fluorescent probe (Fig. S10b), the coexistence of Cu^{2+}, Co^{2+}, Ni^{2+}, Al^{3+}, Cr^{3+}, and Fe^{3+} caused significant interference for the

Table 1 Comparison of the properties of some recently dual fluorescent probes for Zn^{2+} & Mg^{2+} and this work.

Structure of chemosensor	Tested Media	Excitation/ Emission(nm)	LOD (nM)	Ref.
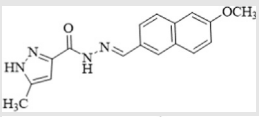	Acetonitrile/H_2O tris-HCl, (7:3, v/v)	370/456 (Zn) 370/ 472 (Mg)	220 (Zn) 390 (Mg)	(Alam, et al., 2014)
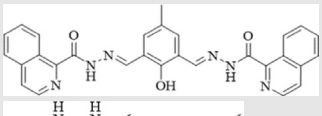	DMF/H_2O(9:1, v/v, PBS buffer, pH7.4) (Zn) Acetonitrile (Mg)	460/536 (Zn) 350/ 560 (Mg)	307 (Zn) 297 (Mg)	(Dhara, et al., 2016)
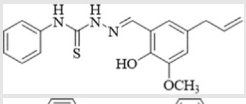	H_2O	323/478 (Zn) 323/ 458 (Mg)	59.4 (Zn) 89.1 (Mg)	(Patil, et al., 2018)
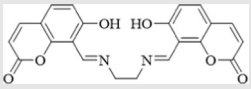	DMF/H_2O (1:4, v/v) (Zn) DMF (Mg)	450/558 (Zn) 350/ 430 (Mg)	53 (Zn) 33 (Mg)	(Li, et al., 2016)
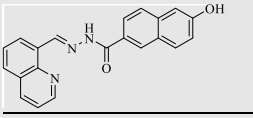	DMSO-H_2O (4:1, v/v) (Zn) ethanol-H_2O (9:1, v/v) (Mg)	400/538 (Zn) 385/ 527 (Mg)	45.1 (Zn) 14.7 (Mg)	This work

QN62-Mg^{2+} complex. Fluorescence quenching was possibly due to the strong complexation abilities or paramagnetic quenching properties of the interfering ions or high Lewis acidity (Wang, et al., 2021; Gao, et al., 2020; Zhou, et al., 2010; Komatsu, et al., 2007; Erdemir and Kocyigit, 2016). Additionally, we attempted to find the lowest concentration of interfering ions that would have a minimal influence on the determination of Zn^{2+}/Mg^{2+}. The experimental results were illustrated in Figs. S10c and Fig. S10d.

3.3. Binding studies

The sharp changes in the optical response of **QN62** before and after Zn^{2+}/Mg^{2+} addition revealed the formation of new species, **QN62**-Zn^{2+} and **QN62**-Mg^{2+} complexes. Because **QN62** contained imine N, quinoline N, carbamoyl O, and phenolic hydroxyl O moieties, **QN62** could utilize these binding sites to coordinate with Zn^{2+}/Mg^{2+}. To explore the binding stoichiometry of **QN62** with Zn^{2+}/Mg^{2+}, the Job's plot based on the emission intensity was studied (Fig. S11). When the value of $[M^{2+}]/[M^{2+}$ + **QN62**] was 0.5, the fluorescence intensity reached a maximum, indicating the formation of 1:1 stoichiometric complexes between **QN62** and Zn^{2+}/Mg^{2+}. The stoichiometry of the complexes was further confirmed by the HR-MS spectral technique. The molecular ion peak *m*/*z* values of the **QN62**-Zn^{2+} and **QN62**-Mg^{2+} complexes were calculated to be 404.0377 and 364.0936, respectively, against experimental values of 404.0381 [**QN62** + Zn^{2+} - H]$^+$ and 364.1054 [**QN62** + Mg^{2+} - H]$^+$ (Fig. S12).

^{1}H NMR titration experiments were performed in DMSO d_6 to understand the binding mode of the **QN62** compound toward Zn^{2+} (Fig. 5). With the gradual addition of Zn^{2+} ions, the amide –NH-C(=O) signal (H_b) of **QN62** at 10.148 ppm slowly disappeared, while a new sharp signal at 9.372 ppm appeared, indicated that the amide converted to the enol-imine tautomeric form. With the addition of 1.0 equiv. of Zn^{2+}, the proton signals of phenolic hydroxyl (H_a) at 12.202 ppm and enol (H_e) at 9.372 ppm disappeared, suggesting that deprotonation of the phenolic hydroxyl and enol in the amide groups occurred when the **QN62** compound coordinated with Zn^{2+}. The upfield signal shift of naphthalene hydrogens was possibly related to the increase in electron density caused by the deprotonation of the phenolic hydroxyl group (Dhara, et al., 2016). In addition, the peak of the imine (H_c) shifted upfield from 9.807 to 9.057 ppm, which could be possibly explained by the ICT effect (Kim and Kim, 2021). However, the signal at 9.017 ppm corresponding to the 2′-position of quinoline (H_d) shifted to 9.155 and the other protons of quinoline also underwent a different extent downfield shift, implying that quinoline N was involved in the coordination reaction between **QN62** and Zn^{2+}. These results indicated that **QN62** could chelate with Zn^{2+} through expected binding sites. Considering that enolic O1 and phenolic hydroxyl O2 were located at the 2- and 6-positions of the naphthalene ring, deprotonated enolic O1 and phenolic hydroxyl O2 in one ligand molecule could not be coordinated to the same zinc ion center. The proposed binding mode of the **QN62** probe with Zn^{2+} was shown in Scheme 2. Zinc ions was coordinated with two N atoms (quinoline N1, imine N2) and one O atom (deprotonated enolic O1) from one **QN62** ligand molecule, and one deprotonated phenolic hydroxyl O2^i of the adjacent other **QN62** ligand.

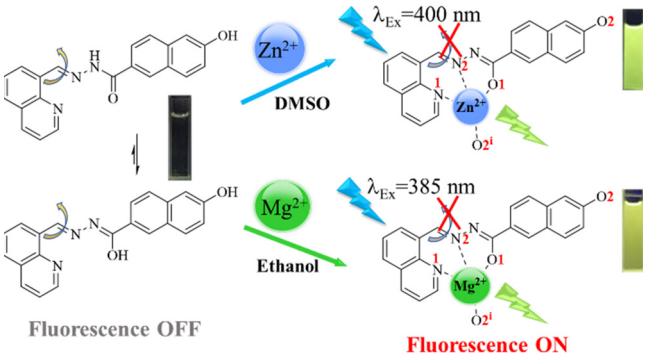

Scheme 2 Plausible binding mode of **QN62** for Zn^{2+} and Mg^{2+}.

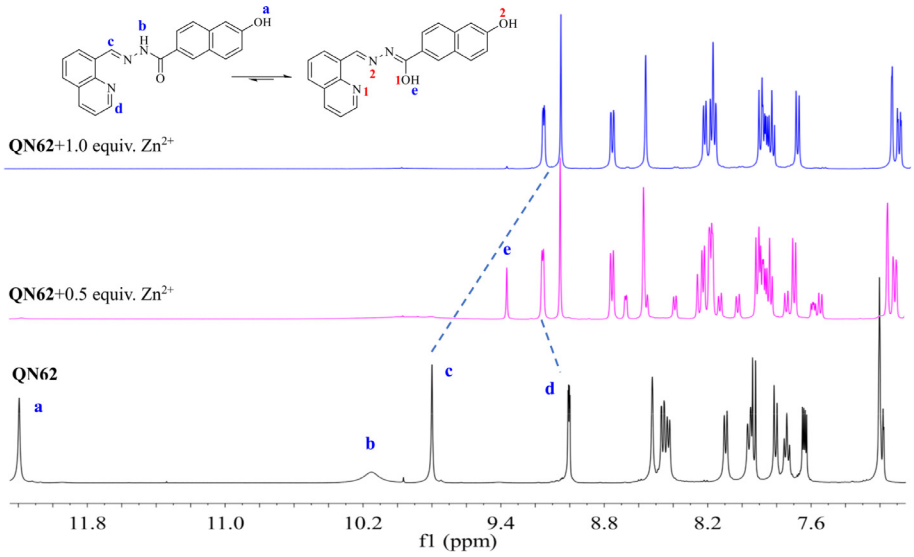

Fig. 5 ^{1}H NMR titration of **QN62** with Zn^{2+} in DMSO d_6.

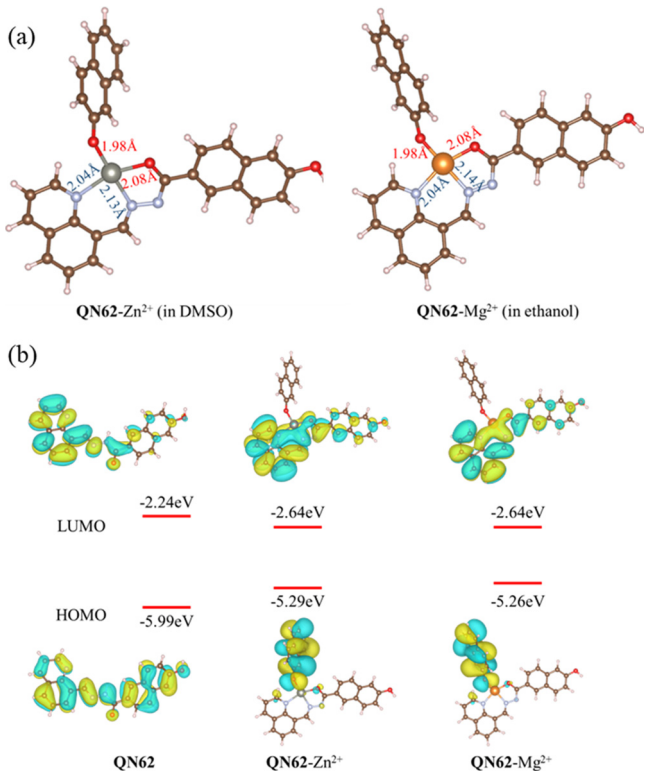

Fig. 6 (a) Optimized structures of the complexes **QN62**-Zn^{2+} and **QN62**-Mg^{2+}. (b) Frontier molecular orbitals of **QN62**, **QN62**-Zn^{2+} and **QN62**-Mg^{2+}.

To further confirm the binding mode between **QN62** and Zn^{2+}/Mg^{2+}, optimized structures of **QN62**-Zn^{2+} and **QN62**-Mg^{2+} were obtained by DFT calculations at the B3LYP/6-31G+ (d,p) level using the Gaussian 16 program (Becke, 1993; Frisch, et al., 2016). In the calculation process, the PCM model was adopted to consider the solvent effect of DMSO and ethanol (Tomasi, et al., 2005). As shown in Fig. 6a, the zinc or magnesium atoms in the optimized complexes coordinated with the deprotonated enol oxygen, imine nitrogen, and nitrogen of quinoline provided by one ligand molecule, and the oxygen of the deprotonated phenolic hydroxyl group of the adjacent ligand, resulting in a distorted tetrahedral coordination geometry. The distances of the coordination bond in the two complexes were in the range of 1.98–2.14 Å, which was comparable to previously reported coordination bonds (Withersby, et al., 1999; Bock, et al., 1999; Ezzayani, et al., 2022).

As indicated by the frontier molecular orbital diagrams shown in Fig. 6b, the enol form of **QN62** had nearly a planar conformation, which could provide π-conjugation and ICT from the donor part (naphthalene ring) to the acceptor part (quinoline unit and acylhydrazone unit) (Li, et al., 2016). In compound **QN62**, the π-electrons of the HOMO were localized over almost the entire molecule, while the π-electrons of the LUMO were restricted to the quinoline unit and the coordination sites. Thus, **QN62** possessed ICT characteristics from the naphthalene ring to the coordination sites. In the energy-optimized structures of **QN62**-Zn^{2+} and **QN62**-Mg^{2+}, the distribution of π-electrons of HOMO and LUMO were very similar. In the complexes, the π-electrons of HOMO and LUMO were distributed mainly over the donor moiety and the acceptor part, respectively, indicating that the complexes possessed more obvious ICT characteristics than the free **QN62** probe. These results showed that the binding of Zn^{2+}/Mg^{2+} to the ligand further encouraged the ICT process by increasing the electron withdrawal ability of the acceptor part (Hossain, et al., 2017). When Zn^{2+}/Mg^{2+} coordinated with **QN62**, the energy gaps decreased, corresponding to the red shift of the

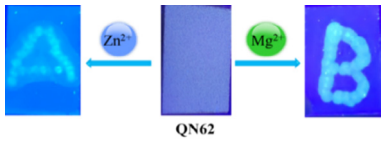

Fig. 8 Photograph of the silica-gel plates containing **QN62** for the detection of Zn^{2+} and Mg^{2+} under UV light (365 nm).

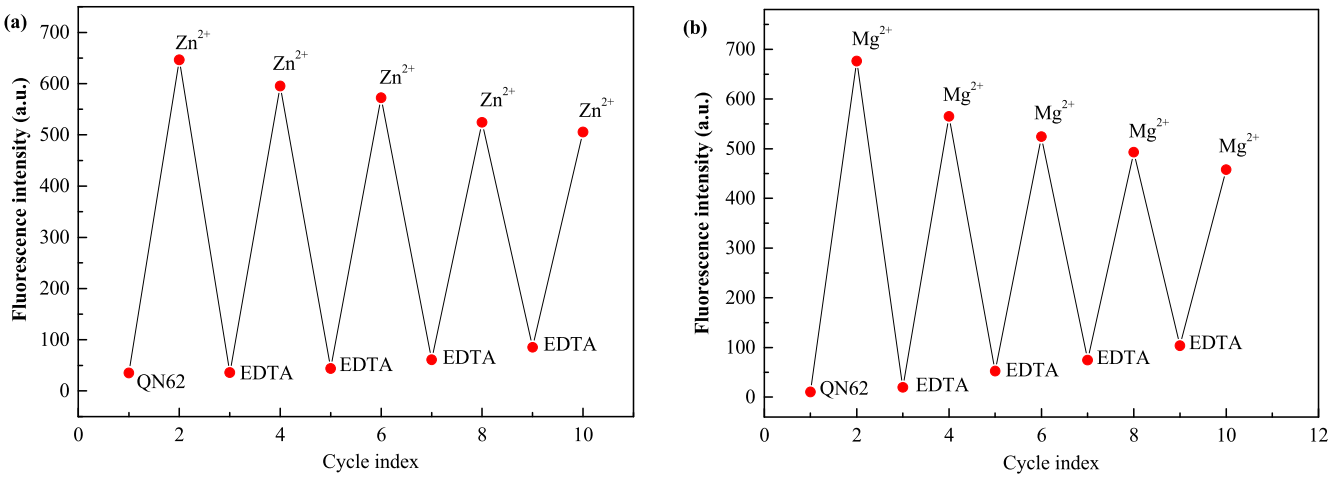

Fig. 7 (a) Reversible changes in fluorescence intensity of **QN62-** (20 μM) at 532 nm upon alternate addition of Zn^{2+} and EDTA in DMSO-H_2O (4:1, v/v). (b) Reversible changes in fluorescence intensity of **QN62** (20 μM) at 527 nm upon alternate addition of Mg^{2+} and EDTA in ethanol-H_2O (9:1, v/v).

Table 2 Recoveries of Zn^{2+} and Mg^{2+} spiked in real water samples using QN62 (n = 3).

Source of samples	Zn^{2+}			Mg^{2+}		
	Added (μM)	Found (μM)	Recovery (%) ± SD	Added (μM)	Found (μM)	Recovery (%) ± SD
Tap water	5.00	4.84	96.80 ± 4.54	5.00	5.29	105.80 ± 3.30
	10.00	9.88	98.80 ± 2.94	10.00	10.16	101.60 ± 2.71
	15.00	15.14	100.93 ± 2.50	15.00	15.10	100.67 ± 1.88
Bottled water	5.00	4.94	98.80 ± 3.26	5.00	5.35	107.00 ± 3.19
	10.00	9.85	98.50 ± 2.16	10.00	10.31	103.10 ± 2.38
	15.00	14.88	99.20 ± 2.05	15.00	15.33	102.20 ± 1.26

UV–vis absorption bands, and the theoretical calculations supported the originally designed concept.

Based on the experimental results and theoretical calculations, we speculated on the response mechanism of **QN62** for Zn^{2+}/Mg^{2+} (Scheme 2). Before the addition of Zn^{2+}/Mg^{2+}, the weak fluorescence of the **QN62** chemosensor was due to the synergistic contribution of the C═N isomerization and the ICT process. With the introduction of Zn^{2+}/Mg^{2+} to the **QN62** system, the binding sites participated in the coordination of **QN62** with Zn^{2+}/Mg^{2+}, which further promoted the ICT process and prevented C═N isomerization, resulting in a significant fluorescence enhancement.

3.4. Reversibility of the chemosensor QN62

The reversibility of the detection process was further evaluated by alternating the addition of Zn^{2+}/Mg^{2+} and ethylenediaminetetraacetic acid (EDTA) in the **QN62** solutions (Fig. 7). Upon the addition of EDTA to the **QN62**-Zn^{2+}/**QN62**-Mg^{2+} sensing solutions, the fluorescence intensity displayed a significant decrease and approached its original value, suggesting that EDTA could complex Zn^{2+}/Mg^{2+} from the complexes and release free **QN62**. With the re-addition of Zn^{2+}/Mg^{2+}, the emission signals recovered, and this reversible cycle was repeated five times with a small emission signal

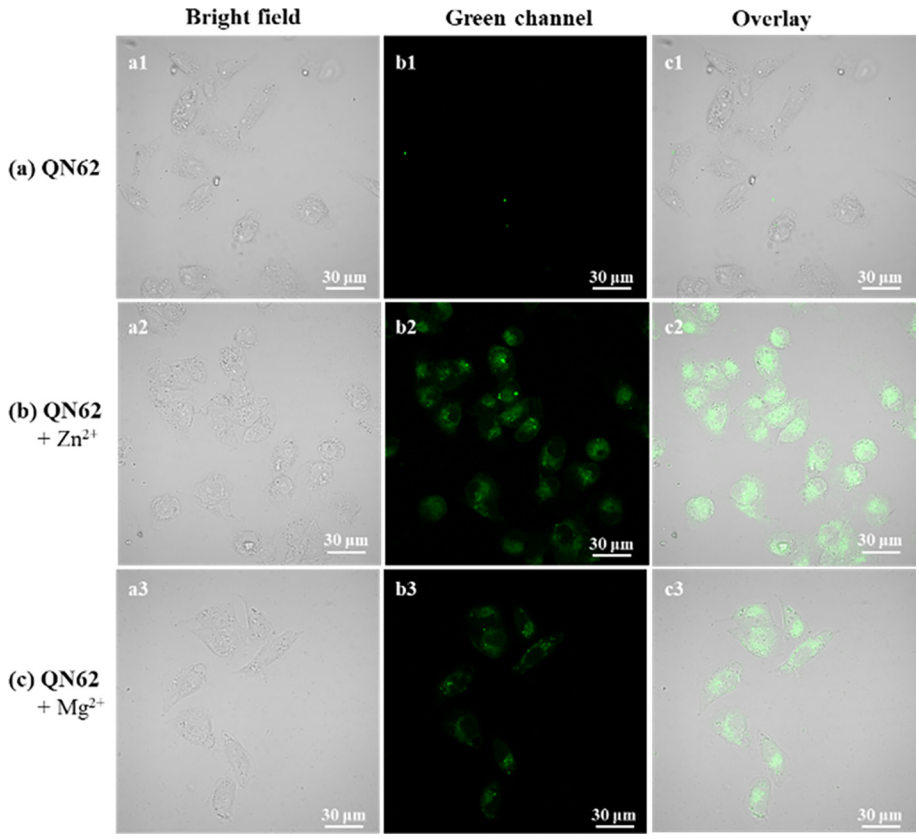

Fig. 9 Bioimaging of exogenous Zn^{2+} and Mg^{2+} in MCF-7 cells with **QN62** (10 μM). (a) Cells stained with **QN62** for 30 min. (b) Cells treated with **QN62** and then with 10 μM Zn^{2+} for 30 min. (c) Cells treated with **QN62** and then with 10 μM Mg^{2+} for 30 min. a1-a3: Bright field; b1-b3: Green channel; c1-c3: Merged images. Green channel: λ_{ex} = 405 nm and collection: 500–550 nm.

decay. The results indicated that **QN62** served as a reversible chemosensor for Zn^{2+}/Mg^{2+} detection.

3.5. Application of chemosensor QN62 in test strip, water samples and cell imaging

To expand the potential practicability of **QN62**, we attempted to recognize Zn^{2+} and Mg^{2+} using silica-gel plates. Silica-gel plates were prepared by immersion in **QN62** solution for a few seconds and then air-dried. Subsequently, the plates were successively treated with Zn^{2+} or Mg^{2+} by using the micro-capillary. We found that silica-gel plates immersed with **QN62** displayed no fluorescence under UV light (Fig. 8). After micro-capillary treatment with Zn^{2+} or Mg^{2+}, the silica-gel plates showed yellowish-green or yellow fluorescence. These findings suggested that the silica-gel plates made from **QN62** could provide a convenient device for the on-site monitoring of Zn^{2+} and Mg^{2+}.

To evaluate the applicability of the **QN62** compound in the samples, we carried out recovery tests using water samples from the campus area. Different concentrations of Zn^{2+}/Mg^{2+} were added to water samples containing **QN62**. The experimental results showed that all the samples had acceptable recoveries with low standard deviation (SD) values, which illustrated the practical application of the **QN62** chemosensor for detecting Zn^{2+} and Mg^{2+} in water samples (Table 2).

Cell imaging experiments were carried out to investigate whether **QN62** could detect intracellular Zn^{2+} and Mg^{2+}, and MCF-7 cells were selected. As shown in Fig. 9, the cells treated with free **QN62** (10 μM) showed negligible fluorescence. After incubation with Zn^{2+}/Mg^{2+} (10 μM), green fluorescence was observed, and the merged images showed that the fluorescence signal was located in the intracellular region. The cell imaging results suggested that the **QN62** chemosensor could sense intracellular Zn^{2+} and Mg^{2+}.

4. Conclusions

In this study, a new dual-functional chemosensor **QN62** based on 6-hydroxy-2-naphthoic hydrazide moieties was successfully designed, synthesized, and characterized by standard techniques and single-crystal X-ray crystallography. **QN62** exhibited simultaneous turn-on fluorescence for Zn^{2+} in DMSO-H_2O (4:1, v/v) solution and Mg^{2+} in ethanol-H_2O (9:1, v/v) solution. Moreover, the recognition progress induced a rapid color change from colorless to yellowish-green or yellow under UV light (365 nm), which was easily visible to the naked eye. After the addition of Zn^{2+} or Mg^{2+} to the corresponding detection system, the fluorescence enhancement response was observed, which could be associated with the coordination of target ions, promoting intramolecular charge transfer (ICT) and preventing C═N isomerization. The limits of detection of **QN62** for Zn^{2+} (32.3 nM) and Mg^{2+} (16.1 nM) were sufficiently low compared to recent literature reports. The detection mechanism was reasonably speculated based on analysis of the Job's plot, HR-MS, ^{1}H NMR, and theoretical calculations. The reversibility experiments indicated that **QN62** could be recycled simply through EDTA treatment. Visual and rapid identification of Zn^{2+} and Mg^{2+} was successfully achieved utilizing silica-gel plates made from the **QN62** chemosensor. The practical applicability of the **QN62** chemosensor in real sample analysis was validated by the addition of Zn^{2+}/Mg^{2+} in water samples. Furthermore, the **QN62** chemosensor could be effectively used for the bioimaging of Zn^{2+} and Mg^{2+} in cells. Based on these results, the **QN62** chemosensor could be used as an addendum in the field of multi-analyte solvent-dependent sensing.

Declaration of Competing Interest

The authors declare the following financial interests/personal relationships which may be considered as potential competing interests: Weiwu Song, Zengchen Liu, GuangLu Liu reports financial support was provided by the National Natural Science Foundation of China. Chunxiang Zhao reports administrative support was provided by the Key Scientific and Technological Project of Zhoukou City.

Acknowledgements

The authors greatly acknowledge the National Natural Science Foundation of China (Grant No. 81803388, No. 31902419, No. 21701203) and the Key Scientific and Technological Project of Zhoukou City (2021GG01011) for the financial support of our work. We thank LetPub (http://www.letpub.com) for linguistic assistance during the preparation of this manuscript, and thank Dr. Yali Cui for the assistance in cell imaging.

Appendix A. Supplementary material

Supplementary data to this article can be found online at https://doi.org/10.1016/j.arabjc.2023.104603.

References

Ahmed, N., Zareen, W., Zhang, D., Yang, X., Ye, Y., 2022. Irreversible coumarin based fluorescent probe for selective detection of Cu^{2+} in living cells. Spectrochim. Acta, Part A 264,. https://doi.org/10.1016/j.saa.2021.120313 120313.

Alam, R., Mistri, T., Katarkar, A., Chaudhuri, K., Mandal, S.K., Khuda-Bukhsh, A.R., Das, K.K., Ali, M., 2014. A novel chromo- and fluorogenic dual sensor for Mg^{2+} and Zn^{2+} with cell imaging possibilities and DFT studies. Analyst 139, 4022–4030. https://doi.org/10.1039/c3an02347h.

Alam, R., Mistri, T., Bhowmick, R., Katarkar, A., Chaudhuri, K., Ali, M., 2016. ESIPT blocked CHEF based differential dual sensor for Zn^{2+} and Al^{3+} in a pseudo-aqueous medium with intracellular bio-imaging applications and computational studies. RSC Adv. 6, 1268–1278. https://doi.org/10.1039/c5ra18424j.

Anbu, S., Ravishankaran, R., Guedes Da Silva, M.F., Karande, A.A., Pombeiro, A.J., 2014. Differentially selective chemosensor with fluorescence off-on responses on Cu^{2+} and Zn^{2+} ions in aqueous media and applications in pyrophosphate sensing, live cell imaging, and cytotoxicity. Inorg. Chem. 53, 6655–6664. https://doi.org/10.1021/ic500313m.

Aysha, T.S., Mohamed, M.B.I., El-Sedik, M.S., Youssef, Y.A., 2021. Multi-functional colorimetric chemosensor for naked eye recognition of Cu^{2+}, Zn^{2+} and Co^{2+} using new hybrid azo-pyrazole/pyrrolinone ester hydrazone dye. Dyes Pigm. 196. https://doi.org/10.1016/j.dyepig.2021.109795.

Becke, A.D., 1993. Density-functional thermochemistry. III. the role of exact exchange. J. Chem. Phys. 98, 5648–5652. https://doi.org/10.1063/1.464913.

Bock, C.W., Katz, A.K., Markham, G.D., Glusker, J.P., 1999. Manganese as a replacement for magnesium and zinc functional comparison of the divalent ions. J. Am. Chem. Soc. 121, 7360–7372. https://doi.org/10.1021/ja9906960.

Brandenburg, K, 2012. DIAMOND. Visual crystal structure information System. Version 3.2i; Crystal impact. Bonn, Germany. http://www.crystalimpact.com.

Bumagina, N.A., Antina, E.V., Krasovskaya, Z.S., Berezin, M.B., Ksenofontov, A.A., Vyugin, A.I., Semeikin, A.S., 2022. Dipyrro-

methene chromo-fluorogenic chemosensors for quantitative detection and express analysis of Zn^{2+} ions. J. Mol. Liq. 345. https://doi.org/10.1016/j.molliq.2021.117834.

Bush, A.I., Pettingell, W.H., Multhaup, G., Paradis, M.D., Vonsattel, J.P., Gusella, J.F., Beyreuther, K., Masters, C.L., Tanzi, R.E., 1994. Rapid induction of Alzheimer A beta amyloid formation by zinc. Science 265, 1464–1467. https://doi.org/10.1126/science.8073293.

Dhara, A., Guchhait, N., Mukherjee, I., Mukherjee, A., Chandra Bhattacharya, S., 2016. A novel pyrazole based single molecular probe for multi-analyte (Zn^{2+} and Mg^{2+}) detection in human gastric adenocarcinoma cells. RSC Adv. 6, 105930–105939. https://doi.org/10.1039/c6ra22869k.

Ding, Y., Zhao, C., Zhang, P., Chen, Y., Song, W., Liu, G., Liu, Z., Yun, L., Han, R., 2021. A novel quinoline derivative as dual chemosensor for selective sensing of Al^{3+} by fluorescent and Fe^{2+} by colorimetric methods. J. Mol. Struct. 1231. https://doi.org/10.1016/j.molstruc.2021.129965.

Djouhra, A., Ali, O., Ramiro, R.R., Emilia, M., 2017. A selective naked-eye chemosensor derived from 2-methoxybenzylamine and 2,3-dihydroxybenzaldehyde - synthesis, spectral characterization and electrochemistry of its bis-bidentates Schiff bases metal complexes. Spectrochim. Acta, Part A 184, 299–307. https://doi.org/10.1016/j.saa.2017.05.022.

Dong, Y., Fan, R., Chen, W., Wang, P., Yang, Y., 2017. A simple quinolone Schiff-base containing CHEF based fluorescence 'turn-on' chemosensor for distinguishing Zn^{2+} and Hg^{2+} with high sensitivity, selectivity and reversibility. Dalton Trans. 46, 6769–6775. https://doi.org/10.1039/c7dt00956a.

Erdemir, S., Kocyigit, O., 2016. Anthracene excimer-based "turn on" fluorescent sensor for Cr^{3+} and Fe^{3+} ions: Its application to living cells. Talanta 158, 63–69. https://doi.org/10.1016/j.talanta.2016.05.017.

Ezzayani, K., Khelifa, A.B., Guesmi, A., Hamadi, N.B., El-Fattah, W. A., Nasri, H., 2022. Application of a new synthesized magnesium porphyrin complex in the degradation of methylene blue dye. J. Mol. Struct. 1258. https://doi.org/10.1016/j.molstruc.2022.132663.

Farruggia, G., Iotti, S., Prodi, L., Montalti, M., Zaccheroni, N., Savage, P.B., Trapani, V., Sale, P., Wolf, F.I., 2006. 8-Hydroxyquinoline derivatives as fluorescent sensors for magnesium in living cells. J. Am. Chem. Soc. 128, 344–350. https://doi.org/10.1021/ja056523u.

Frisch, M.J.; Trucks, G.W.; Schlegel, H.B.; Scuseria, G.E.; Robb, M. A.; Cheeseman, J.R.; Scalmani, G.; Barone, V.; Petersson, G.A.; Nakatsuji, H.; Li, X.; Caricato, M.; Marenich, A.V.; Bloino, J.; Janesko, B.G.; Gomperts, R.; Mennucci, B.; Hratchian, H.P.; Ortiz, J.V.; Izmaylov, A.F.; Sonnenberg, J.L.; Williams-Young, D.; Ding, F.; Lipparini, F.; Egidi, F.; Goings, J.; Peng, B.; Petrone, A.; Henderson, T.; Ranasinghe, D.; Zakrzewski, V.G.; Gao, J.; Rega, N.; Zheng, G.; Liang, W.; Hada, M.; Ehara, M.; Toyota, K.; Fukuda, R.; Hasegawa, J.; Ishida, M.; Nakajima, T.; Honda, Y.; Kitao, O.; Nakai, H.; Vreven, T.; Throssell, K.; Montgomery, J.A., Jr.; Peralta, J.E.; Ogliaro, F.; Bearpark, M.J.; Heyd, J.J.; Brothers, E.N.; Kudin, K.N.; Staroverov, V.N.; Keith, T.A.; Kobayashi, R.; Normand, J.; Raghavachari, K.; Rendell, A.P.; Burant, J.C.; Iyengar, S.S.; Tomasi, J.; Cossi, M.; Millam, J.M.; Klene, M.; Adamo, C.; Cammi, R.; Ochterski, J.W.; Martin, R.L.; Morokuma, K.; Farkas, O.; Foresman, J.B.; Fox, D.J., 2016. Gaussian 16, Revision C.01, Gaussian, Inc.: Wallingford CT.

Fu, Z.H., Qin, J.C., Wang, Y.W., Peng, Y., Zhang, Y.M., Zhao, D.M., Zhang, Z.H., 2021. A quinoline-based chromogenic and ratiometric fluorescent probe for selective detection of Mg^{2+} ion: Design, synthesis and its application in salt lake brines and bioimaging. Dyes Pigm. 185. https://doi.org/10.1016/j.dyepig.2020.108896.

Gao, L.L., Li, S.P., Wang, Y., Wu, W.N., Zhao, X.L., Li, H.J., Xu, Z. H., 2020. Quinoline-based hydrazone for colorimetric detection of Co^{2+} and fluorescence turn-on response of Zn^{2+}. Spectrochim. Acta, Part A 230,. https://doi.org/10.1016/j.saa.2020.118025 118025.

Geng, R., Tang, H., Ma, Q., Liu, L., Feng, W., Zhang, Z., 2022. Bimetallic Ag/Zn-ZIF-8: An efficient and sensitive probe for Fe^{3+} and Cu^{2+} detection. Colloids. Surf., A 632. https://doi.org/10.1016/j.colsurfa.2021.127755.

Gogoi, A., Samanta, S., Das, G., 2014. A benzothiazole containing CHEF based fluorescence turn-ON sensor for Zn^{2+} and Cd^{2+} and subsequent sensing of $H_2PO_4^-$ and $P_4O_7^{4-}$ in physiological pH. Sens. Actuators, B 202, 788–794. https://doi.org/10.1016/j.snb.2014.06.012.

Goncalves, H.M.R., Tavares, I.S., Neves, S.A.F., Fontes, R., Duarte, A.J., 2022. Turn-on, photostable, nontoxic and specific, iron(II) sensor. Spectrochim. Acta, Part A 265. https://doi.org/10.1016/j.saa.2021.120380.

Hazra, A., Roy, A., Mukherjee, A., Maiti, G.P., Roy, P., 2018. Remarkable difference in Al^{3+} and Zn^{2+} sensing properties of quinoline based isomers. Dalton Trans. 47, 13972–13989. https://doi.org/10.1039/c8dt02856g.

Hossain, S.M., Singh, K., Lakma, A., Pradhan, R.N., Singh, A.K., 2017. A schiff base ligand of coumarin derivative as an ICT-Based fluorescence chemosensor for Al^{3+}. Sens. Actuators, B 239, 1109–1117. https://doi.org/10.1016/j.snb.2016.08.093.

Hu, J.H., Li, J.B., Sun, Y., Pei, P.X., Qi, J., 2017. A turn-on fluorescent chemosensor based on acylhydrazone for sensing of Mg^{2+} with a low detection limit. RSC Adv. 7, 29697–29701. https://doi.org/10.1039/c7ra04462c.

Immanuel David, C., Jayaraj, H., Prabakaran, G., Velmurugan, K., Parimala Devi, D., Kayalvizhi, R., Abiram, A., Rajesh Kannan, V., Nandhakumar, R., 2022. A photoswitchable "turn-on" fluorescent chemosensor: Quinoline-naphthalene duo for nanomolar detection of aluminum and bisulfite ions and its multifarious applications. Food Chem. 371,. https://doi.org/10.1016/j.foodchem.2021.131130 131130.

Jana, A., Das, B., Mandal, S.K., Mabhai, S., Khuda-Bukhsh, A.R., Dey, S., 2016. Deciphering the CHEF-PET-ESIPT liaison mechanism in a Zn^{2+} chemosensor and its applications in cell imaging study. New J. Chem. 40, 5976–5984. https://doi.org/10.1039/c6nj00234j.

Jiang, K., Luo, S.H., Pang, C.M., Wang, B.W., Wu, H.Q., Wang, Z. Y., 2019. A functionalized fluorochrome based on quinoline-benzimidazole conjugate: from facile design to highly sensitive and selective sensing for picric acid. Dyes Pigm. 162, 367–376. https://doi.org/10.1016/j.dyepig.2018.10.041.

Khan, S., Muhammad, M., Al-Saidi, H.M., Hassanian, A.A., Alharbi, W., Alharbi, K.H., 2022. Synthesis, characterization and applications of schiff base chemosensor for determination of Cu^{2+} ions. J. Saudi Chem. Soc. 26. https://doi.org/10.1016/j.jscs.2022.101503.

Khan, S., Muhammad, M., Algethami, J.S., Al-Saidi, H.M., Almahri, A., Hassanian, A.A., 2022. Synthesis, Characterization and Applications of Schiff Base Chemosensor for Determination of Cr(III) Ions. J. Fluoresc. 32, 1889–1898. https://doi.org/10.1007/s10895-022-02990-7.

Kim, T., Kim, J., 2021. Color-tunable indolizine-based fluorophores and fluorescent pH sensor. Molecules 27. https://doi.org/10.3390/molecules27010012.

Kolcu, F., Kaya, İ., 2022. Carbazole-based Schiff base: A sensitive fluorescent 'turn-on' chemosensor for recognition of Al(III) ions in aqueous-alcohol media. Arabian J. Chem. 15. https://doi.org/10.1016/j.arabjc.2022.103935.

Komatsu, K., Urano, Y., Kojima, H., Nagano, T., 2007. Development of an iminocoumarin-based zinc sensor suitable for ratiometric fluorescence imaging of neuronal zinc. J. Am. Chem. Soc. https://doi.org/10.1021/ja072432g.

Kumar, M., Puri, A., 2012. A review of permissible limits of drinking water. Indian J. Occup. Environ. Med. 16, 40–44. https://doi.org/10.4103/0019-5278.99696.

Li, Y., Chen, J., Chu, T.S., 2016. Sensing mechanism for a fluorescent off-on chemosensor for cyanide anion. J. Lumin. 179, 203–210. https://doi.org/10.1016/j.jlumin.2016.07.024.

Li, N.N., Ma, Y.Q., Sun, X.J., Li, M.Q., Zeng, S., Xing, Z.Y., Li, J.L., 2019. A dual-function probe based on naphthalene for fluorescent turn-on recognition of Cu^{2+} and colorimetric detection of Fe^{3+} in neat H_2O. Spectrochim. Acta, Part A 210, 266–274. https://doi.org/10.1016/j.saa.2018.11.031.

Li, L., Shen, Y., Zhao, Y., Ma, L., Zeng, X., Redshaw, C., Wei, G., 2016. A single chemosensor for multiple analytes: Fluorogenic and ratiometric absorbance detection of Zn^{2+}, Mg^{2+} and F^{-}, and its cell imaging. Sens. Actuators, B 226, 279–288. https://doi.org/10.1016/j.snb.2015.11.126.

Liao, Z., Liu, Y., Han, S.F., Wang, D., Zheng, J.Q., Zheng, X.J., Jin, L.P., 2017. A novel acylhydrazone-based derivative as dual-mode chemosensor for Al^{3+}, Zn^{2+} and Fe^{3+} and its applications in cell imaging. Sens. Actuators, B 244, 914–921. https://doi.org/10.1016/j.snb.2017.01.074.

Maity, S.B., Bharadwaj, P.K., 2014. A molecular dual fluorescence-ON probe for Mg^{2+} and Zn^{2+}: higher selectivity towards Mg^{2+} over Zn^{2+} in a mixture. J. Lumin. 155, 21–26. https://doi.org/10.1016/j.jlumin.2014.06.020.

Maity, D., Mukherjee, A., Mandal, S.K., Roy, P., 2019. Modulation of fluorescence sensing properties of quinoline-based chemosensor for Zn^{2+}: application in cell imaging studies. J. Lumin. 210, 508–518. https://doi.org/10.1016/j.jlumin.2019.02.046.

Maret, W., 2015. Analyzing free zinc(II) ion concentrations in cell biology with fluorescent chelating molecules. Metallomics 7, 202–211. https://doi.org/10.1039/c4mt00230j.

Matsui, Y., Sadhu, K.K., Mizukami, S., Kikuchi, K., 2017. Highly selective tridentate fluorescent probes for visualizing intracellular Mg^{2+} dynamics without interference from Ca^{2+} fluctuation. Chem. Commun. 53, 10644–10647. https://doi.org/10.1039/c7cc06141b.

Mohamed, M.B.I., El-Sedik, M.S., Youssef, Y.A., Mohamed, N.A., Aysha, T.S., 2022. New stilbene-biscarbothioamide based colorimetric chemosensor and turn on fluorescent probe for recognition of Hg^{2+} cation. J Photochem. Photobiol. A 433. https://doi.org/10.1016/j.jphotochem.2022.114206.

Mohanasundaram, D., Bhaskar, R., Gangatharan Vinoth Kumar, G., Rajesh, J., Rajagopal, G., 2021. A quinoline based Schiff base as a turn-on fluorescence chemosensor for selective and robust detection of Cd^{2+} ion in semi-aqueous medium. Microchem. J. 164. https://doi.org/10.1016/j.microc.2021.106030

Moreno, J.L., Bastida, F., Ros, M., Hernández, T., García, C., 2009. Soil organic carbon buffers heavy metal contamination on semiarid soils: effects of different metal threshold levels on soil microbial activity. Eur. J. Soil Biol. 45, 220–228. https://doi.org/10.1016/j.ejsobi.2009.02.004.

Musikavanhu, B., Muthusamy, S., Zhu, D., Xue, Z., Yu, Q., Chiyumba, C.N., Mack, J., Nyokong, T., Wang, S., Zhao, L., 2022. A simple quinoline-thiophene Schiff base turn-off chemosensor for Hg^{2+} detection: spectroscopy, sensing properties and applications. Spectrochim. Acta, Part A 264,. https://doi.org/10.1016/j.saa.2021.120338 120338.

Patil, M., Keshav, K., Kumawat, M.K., Bothra, S., Sahoo, S.K., Srivastava, R., Rajput, J., Bendre, R., Kuwar, A., 2018. Monoterpenoid derivative based ratiometric fluorescent chemosensor for bioimaging and intracellular detection of Zn^{2+} and Mg^{2+} ions. J. Photochem. Photobiol. A 364, 758–763. https://doi.org/10.1016/j.jphotochem.2018.07.015.

Picci, G., Milia, J., Aragoni, M.C., Arca, M., Coles, S.J., Garau, A., Lippolis, V., Montis, R., Orton, J.B., Caltagirone, C., 2021. Switching-on fluorescence by copper(II) and basic anions: a case study with a pyrene-functionalized squaramide. Molecules 26. https://doi.org/10.3390/molecules26051301.

Purkait, R., Mahapatra, A.D., Chattopadhyay, D., Sinha, C., 2019. An azine-based carbothioamide chemosensor for selective and sensitive turn-on-off sequential detection of Zn(II) and $H_2PO_4^-$, live cell imaging and INHIBIT logic gate. Spectrochim. Acta, Part A 207, 164–172. https://doi.org/10.1016/j.saa.2018.09.019.

Roy, A., Nandi, M., Roy, P., 2021. Dual chemosensors for metal ions: a comprehensive review. Trends Anal. Chem. 138. https://doi.org/10.1016/j.trac.2021.116204.

Rurack, K., 2008. Fluorescence quantum yields methods of determination and standards. Springer Ser. Fluoresc. 5, 101–145. https://doi.org/10.1007/4243_2008_019.

Saravana Kumar, S., Selva Kumar, R., Ashok Kumar, S.K., 2020. An "Off-On-Off" type fluorescent chemosensor for the relay detection of Zn^{2+} and $H_2PO_4^-$ in aqueous environment. Inorg. Chim. Acta 502. https://doi.org/10.1016/j.ica.2019.119348.

Sheldrick, G.M., 1997. SHELXL-97. University of Göttingen, Germany, Program for Crystal Structure Refinement.

Shi, Z., Tang, X., Zhou, X., Cheng, J., Han, Q., Zhou, J.A., Wang, B., Yang, Y., Liu, W., Bai, D., 2013. A highly selective fluorescence "turn-on" probe for Cu(II) based on reaction and its imaging in living cells. Inorg. Chem. 52, 12668–12673. https://doi.org/10.1021/ic401865e.

Shyamsivappan, S., Saravanan, A., Vandana, N., Suresh, T., Suresh, S., Nandhakumar, R., Mohan, P.S., 2020. Novel quinoline-based thiazole derivatives for selective detection of Fe^{3+}, Fe^{2+}, and Cu^{2+} ions. ACS Omega 5, 27245–27253. https://doi.org/10.1021/acsomega.0c03445.

Sidqi, M.E., Abdel Aziz, A.A., Abolehasan, A.E., Sayed, M.A., 2022. Photochemical processing potential of a novel Schiff base as a fluorescent probe for selective monitoring of Al^{3+} ions and bioimaging in human cervical cancer HeLa cells. J. Photochem. Photobiol. A, 424. https://doi.org/10.1016/j.jphotochem.2021.113616.

Sivakumar, R., Lee, N.Y., 2021. Paper-based fluorescence chemosensors for metal ion detection in biological and environmental samples. BioChip J. 15, 216–232. https://doi.org/10.1007/s13206-021-00026-z.

Sun, X.J., Liu, T.T., Li, N.N., Zeng, S., Xing, Z.Y., 2020. A novel dual-function probe for recognition of Zn^{2+} and Al^{3+} and its application in real samples. Spectrochim. Acta, Part A 228,. https://doi.org/10.1016/j.saa.2019.117786 117786.

Tomasi, J., Mennucci, B., Cammi, R., 2005. Quantum mechanical continuum solvation models. Chem. Rev. 105, 2999–3093. https://doi.org/10.1021/cr9904009.

Voegelin, A., Pfister, S., Scheinost, A.C., Marcus, M.A., Kretzschmar, R., 2005. Changes in zinc speciation in field soil after contamination with zinc oxide. Environ. Sci. Technol. 39, 6616–6623. https://doi.org/10.1021/es047962g.

Wang, J.T., Pei, Y.Y., Yan, M.Y., Li, Y.G., Yang, G.G., Qu, C.H., Luo, W., Wang, J., Li, Q.F., 2021. A fast-response turn-on quinoline-based fluorescent probe for selective and sensitive detection of zinc(II) and its application. Microchem. J. 160. https://doi.org/10.1016/j.microc.2020.105776.

Wang, Y., Wang, Z.G., Song, X.Q., Chen, Q., Tian, H., Xie, C.Z., Li, Q.Z., Xu, J.Y., 2019. A dual functional turn-on non-toxic chemosensor for highly selective and sensitive visual detection of Mg^{2+} and Zn^{2+}: the solvent-controlled recognition effect and bioimaging application. Analyst 144, 4024–4032. https://doi.org/10.1039/c9an00583h.

Wang, F., Wang, K., Kong, Q., Wang, J., Xi, D., Gu, B., Lu, S., Wei, T., Chen, X., 2021. Recent studies focusing on the development of fluorescence probes for zinc ion. Coord. Chem. Rev. 429. https://doi.org/10.1016/j.ccr.2020.213636.

Wang, Z., Zheng, C., Xu, D., Liao, G., Pu, S., 2022. A fluorescent sensor for Zn^{2+} and Cd^{2+} based on a diarylethene derivative with an indole-2-methylhydrazone moiety. J. Photochem. Photobiol. A, 424. https://doi.org/10.1016/j.jphotochem.2021.113634.

Withersby, M.A., Blake, A.J., Champness, N.R., Cooke, P.A., Hubberstey, P., Li, W.S., Schröder, M., 1999. Solvent control in the synthesis of 3,6-bis(pyridin-3-yl)-1,2,4,5-tetrazine-bridged cad-

mium(II) and zinc(II) coordination polymers. Inorg. Chem. 38, 2259–2266. https://doi.org/10.1021/ic980898h.

Wu, W.N., Mao, P.D., Wang, Y., Zhao, X.L., Xu, Z.Q., Xu, Z.H., Xue, Y., 2018. Quinoline containing acetyl hydrazone: An easily accessible switch-on optical chemosensor for Zn^{2+}. Spectrochim. Acta, Part A 188, 324–331. https://doi.org/10.1016/j.saa.2017.07.020.

Xie, Z., Kong, X., Feng, L., Ma, J., Li, Y., Wang, X., Bao, W., Shi, W., Hui, Y., 2018. A novel highly selective probe with both aggregation-induced emission enhancement and intramolecular charge transfer characteristics for CN^- detection. Sens. Actuators, B 257, 154–165. https://doi.org/10.1016/j.snb.2017.10.167.

Xu, Y., Mao, S., Peng, H., Wang, F., Zhang, H., Aderinto, S.O., Wu, H., 2017. A fluorescent sensor for selective recognition of Al^{3+} based on naphthalimide Schiff-base in aqueous media. J. Lumin. 192, 56–63. https://doi.org/10.1016/j.jlumin.2017.06.023.

Xu, H., Zhang, S., Gu, Y., Lu, H., 2022. Naphthalimide appended isoquinoline fluorescent probe for specific detection of Al^{3+} ions and its application in living cell imaging. Spectrochim. Acta, Part A 265,. https://doi.org/10.1016/j.saa.2021.120364 120364.

Yan, X.J., Gao, Y.Y., Liu, H.B., Qiao, X., Xie, C.Z., Li, Q.Z., Gao, W.Z., Sun, H.B., Xu, J.Y., 2021. A novel double target fluorescence probe for Al^{3+}/Mg^{2+} detection with distinctively different responses and its applications in cell imaging. Spectrochim. Acta, Part A 261,. https://doi.org/10.1016/j.saa.2021.120067 120067.

Zhang, S., Sun, T., Xiao, D., Yuan, F., Li, T., Wang, E., Liu, H., Niu, Q., 2018. A dual-responsive colorimetric and fluorescent chemosensor based on diketopyrrolopyrrole derivative for naked-eye detection of Fe^{3+} and its practical application. Spectrochim. Acta, Part A 189, 594–600. https://doi.org/10.1016/j.saa.2017.09.001.

Zhou, X., Yu, B., Guo, Y., Tang, X., Zhang, H., Liu, W., 2010. Both visual and fluorescent sensor for Zn^{2+} based on quinoline platform. Inorg. Chem. 49, 4002–4007. https://doi.org/10.1021/ic901354x.